Soft Matter

Accepted Manuscript

ROYAL SOCIETY OF CHEMISTRY

www.rsc.org/softmatter

ARTICLE TYPE www. rsc.org/xxxxxx | XXXXXXXX

Driving knots on DNA with AC/DC electric fields: topological friction and memory effects

Marco Di Stefano*[a], Luca Tubiana*[b], Massimiliano Di Ventra[c] and Cristian Micheletti[a]

Received Xth XXXXXXXXXX 20XX, Accepted Xth XXXXXXXXX 20XX
First published on the web Xth XXXXXXXXXX 20XX
DOI: 10.1039/b000000x

Abstract The dynamical properties of entangled polyelectrolytes are investigated theoretically and computationally for a proposed novel micromanipulation setup. Specifically, we investigate the effects of DC and AC electric fields acting longitudinally on knotted DNA chains, modelled as semiflexible chains of charged beads, under mechanical tension. We consider various experimentally accessible values of the field amplitude and frequency as well as several of the simplest knot types. In particular, we consider both torus and twist knots because they are respectively known to be able or unable to slide along macroscopic threads and ropes. Strikingly, this qualitative distinction disappears in this microscopic context because all the considered knot types acquire a systematic drift in the direction of the electric force. Notably, the knot drift velocity and diffusion coefficient in zero field (both measurable also experimentally) can be used to define a characteristic "frictional" lengthscale for the various knot types. This previously unexplored length provides valuable information on the extent of self-interactions in the nominal knotted region. It is finally observed that the motion of a knot can effectively follow the AC field only if the driving period is larger than the knot relaxation time (for which the self-diffusion time provides an upper bound). These results suggests that salient aspects of the intrinsic dynamics of knots in DNA chains could be probed experimentally by means of external, time-dependent electric fields.

1 Introduction

The impact of entanglement, such as knots and links, on the physical properties of biopolymers[1], is attracting increasing interest both for its general connection with polymer theory[2–10] and for its biological[11,12] and technological ramifications[13,14]. However, a still relatively unexplored avenue is the characterization of the dynamics of entangled chains and its relationship with static properties such as the equilibrium knotting probability and the average knot size.

In fact, in the past few years a number of experimental and theoretical studies have dealt with fundamental issues such as classifying the mechanisms leading to the spontaneous formation and untying of knots in biopolymers[15–19], identifying the additional length and time scales of relaxation introduced by the presence of knots in chains and rings[20–23] or the topological friction hindering translocation of polymers through pores[14,24,25], their motion in a channel[26] or the DNA ejection from viral capsids[27,28].

One prototypical context where several of these aspects can be simultaneously observed and analyzed is constituted by knotted molecules under mechanical tension. A classic example is offered by DNA filaments that can be both knotted and stretched by moving the termini in space using optical tweezers[29–31]. These setups have provided considerable insight into the complex interplay of characteristic time-scales[32,33] and length-scales[7] that generally control the spontaneous dynamics of the knotted region, knot lifetimes and ultimately the knotting probability of unconstrained chains[8,19], as well as on the thermodynamic properties of knots[34,35].

Here, to advance our understanding of the stochastic dynamics of knots in polymers we introduce an external electric field acting longitudinally on knotted polyelectrolyte chains under mechanical tension.

Specifically, we consider model knotted DNA chains under mechanical tension and analyze how the knotted region evolves under the action of external DC or AC electric fields with experimentally accessible magnitude and frequency.

It is found that, in the presence of a longitudinal DC electric field, all considered knots acquire a net drift in the direction of the electric force. Interestingly, the drift velocity is comparable for torus and twist knots.

Notably, by using AC electric fields of sufficiently high fre-

[a] *SISSA - Scuola Internazionale Superiore di Studi Avanzati, Via Bonomea 265, 34136 Trieste (Italy).*
[b] *Department of Theoretical Physics, Jožef Stefan Institute, SI-1000 Ljubljana, Slovenia*
[c] *Department of Physics, University of California, San Diego, California 92093-0319, USA*

quency the periodic drift motion of knots can be largely reduced and even suppressed. The cutoff period, identified by measuring the dissipated power, provides a measure for the intrinsic relaxation time for the knot. Only for AC periods longer than this relaxation time, knots can follow and adjust to the periodic reversal of the field. The observed time delay and cutoff period are typical features of complex systems with memory[36].

The robustness of these results, which are obtained using a Debye-Hückel potential to account for the electrostatic screening operated by counterions, is finally verified in a model polyelectrolyte system with explicit counterions.

To the best of our knowledge, the combined application of a tensile force and DC/AC fields has not been previously considered neither for DNA nor for other polyelectrolytes and could be relevant in applicative contexts, such as DNA display and micromanipulation experiments, or DNA sequencing and detection[37]. The present study ought to provide a quantitative insight into the relevant timescales controlling the dynamical evolution of self-entanglement in such systems.

2 Methods

2.1 DNA model

We consider a knotted polyelectrolyte (PE) chain that is mechanically stretched at both termini by a pulling force $\vec{F}_s$ along the z Cartesian axis, whose unit vector we shall indicate with $\hat{z}$. Once the chain is stretched and equilibrated, the two termini are pinned and the chain experiences a spatially-uniform longitudinal external electric field (both DC and AC).

The PE is modeled by a semi-flexible chain of $N = 2000$ beads. Each bead has mass m, electric charge q and diameter σ. The simulations are carried out in a periodic parallelepiped simulation box, whose z-side has length $N\sigma$ while each of the other two sides have length $100\,\sigma$.

The beads interact with the following potential energy:

$$\mathscr{H} = U_{\rm FENE} + U_{\rm KP} + U_{\rm LJ} + U_{\rm DH} + U_{\rm ext} \tag{1}$$

The adjacent beads are connected to each other by FENE bonds:

$$U_{\rm FENE} = -\sum_{i}^{N-1} 15\varepsilon \left(\frac{R_0}{\sigma}\right)^2 \ln\left[1-\left(\frac{d_{i,i+1}}{R_0}\right)^2\right] \tag{2}$$

where $d_{i,i+1} = |\vec{r}_i - \vec{r}_{i+1}|$ is the distance of the bead centers i and $i+1$, $R_0 = 1.5\sigma$ is the maximum bond length and ε is the interaction strength[38]. Triplets of consecutive beads are involved in the Kratky-Porod interaction:

$$U_{\rm KP} = \sum_{i=2}^{N-1} \varepsilon \left(\frac{l_p}{\sigma}\right)\left(1 - \frac{\vec{b}_{i-1}\cdot\vec{b}_i}{\left|\vec{b}_{i-1}\right|\left|\vec{b}_i\right|}\right) \tag{3}$$

where $\vec{b}_i \equiv \vec{r}_{i+1} - \vec{r}_i$ is the ith chain bond. This interaction accounts for the bending rigidity of the chain that is controlled with the nominal persistence length $l_p = 20\sigma$. The truncated and shifted Lennard-Jones interaction prevents chain self-crossing:

$$U_{\rm LJ} = \frac{1}{2}\sum_{(i,j),j\neq i}^{N} 4\varepsilon\left[\left(\frac{\sigma}{d_{i,j}}\right)^{12} - \left(\frac{\sigma}{d_{i,j}}\right)^{6} + \frac{1}{4}\right] \tag{4}$$

applied for distances $d_{i,j} \leq 2^{1/6}\sigma$. The electrostatic self-repulsion is treated with the Debye-Hückel term:

$$U_{\rm DH} = \frac{1}{2}\sum_{(i,j),j\neq i}^{N} \frac{q_i q_j}{4\pi\varepsilon_0\,\varepsilon_r d_{i,j}}\, e^{-\frac{d_{ij}}{\lambda_{DH}}} \tag{5}$$

and acts between all the pairs of beads at distances $d_{i,j} \leq 8\sigma$. $\varepsilon_0\varepsilon_r$ is the permettivity of the medium, κ_B is the Boltzmann constant, T is the temperature and $\lambda_{DH} = (8\pi N_A I l_B)^{-1/2}$ is the Debye-Hückel screening length, where N_A the Avogadro number and I is the solution ionic strength.

The last term in eqn. 1, $U_{\rm ext}$, describes the interactions of the PE chain with the external forces. When studying the free diffusion of knots along the stretched DNA chains without any external field, one simply considers the potential energy associated to the stretching force F_s pulling the two termini in the $-\hat{z}$ and $+\hat{z}$ directions, respectively:

$$U_{\rm ext} \quad = \quad \vec{F}_s\cdot(\vec{r}_1 - \vec{r}_N) \tag{6}$$

where $\vec{F}_s = F_s\hat{z}$. When considering the interaction with a spatially-uniform, but possibly time-dependent, external field $E(t)$, the stretching force is replaced by a constraint which keeps the termini fixed and apart in space (so that the chain cannot move as a whole). The field potential energy is:

$$U_{\rm ext} \quad = \quad \sum_{i=1}^{N} qE(t)\,\hat{z}\cdot\vec{r}_i\ . \tag{7}$$

The chain dynamics is described with an underdamped Langevin equation:

$$m\ddot{\vec{r}} = -\gamma\dot{\vec{r}} - \nabla\mathscr{H} + \vec{\eta}\,(t) \tag{8}$$

where $\langle\eta_\alpha\rangle = 0$ for each Cartesian component $\alpha = x, y, z$ and $\langle\eta_\alpha(t)\,\eta_\beta(t')\rangle = 2\kappa_B T\gamma\delta_{\alpha,\beta}\,\delta_{t,t'}$. The Langevin equation is solved numerically with the LAMMPS simulation package[39], with an integration time step $\Delta t = 0.012\tau_{LJ}$, where $\tau_{LJ} = \sigma\sqrt{m/\varepsilon}$ and with $m/\gamma = 2\tau_{LJ}$, as in Ref.[38].

2.2 Model parameters

The parameters of the model PE are tuned so as to match the nominal properties of a dsDNA filament in water solution ($\varepsilon_r = 80$) with $0.01\,M$ NaCl at $T = 300$K. The effective

charge of the beads, each spanning ~ 8 basepairs, is set equal to $q = -8$e, to account for the $\sim 50\%$ reduction of the nominal phosphate charge due to monovalent counterions[40]. The Bjerrum length is accordingly set to $l_B = e^2/(4\pi\varepsilon_0\varepsilon_r\kappa_B T) = 0.7$nm and the Debye-Hückel screening length is $\lambda = 3$nm. The interaction strength ε is set equal to $\kappa_B T = 4 \cdot 10^{-21} J$ at $T = 300\,K$. The Debye-Hückel potential clearly increases the effective self-avoidance and mechanical rigidity of the chain whose nominal, intrisic, properties are as follows: the bead diameter is equal to the nominal hydrated DNA diameter, $\sigma = 2.5$nm and the persistence length is set equal to $l_p = 50$nm.

Assuming that the beads viscous drag follows Stokes' law one has $\tau_{LJ} = 6\pi\eta\sigma^3/\varepsilon$. For water solutions, where $\eta = 1$ cP, one has $\tau_{LJ} \sim 75$ns so that each integration time step has a duration of $\Delta t \sim 1$ns.

2.3 System setup and simulation details

The initial configuration of the knotted chains were generated by first discretising in about 300 beads a parametric closed knotted configuration obtained from the *MathWorld* Wolfram web resource, next opening it by removing 15-20 beads and finally prolonging the termini with straight segments running in opposite directions, and of equal length appropriate to yield a total of $N = 2000$ beads in the chain.

The obtained configurations are next equilibrated for $1 \cdot 10^8$ integration steps under the action of a longitudinal stretching force of $F_s = 10.0$pN applied at both termini. After this equilibration time, various observables are recorded at fixed stretching force.

When investigating the action of an external longitudinal electric field, E, the stretching force, F_s is replaced by pinning the chain termini. This change of boundary conditions is made necessary as the whole chain would otherwise drift. The ends pinning is introduced on chain configurations previously equilibrated at $F_s = 10.0$pN, so that for $E = 0$ the nominal average chain tension is equal to the stretching force in zero field, 10.0pN.

For each considered condition (various tensile forces in no external field, fixed termini at various DC and AC field) we gathered from a minimum of 3 to a maximum of 10 different production runs each typically covering 10^9 integration steps. The reported values of the average knot length, $\langle l_k \rangle$ and its estimated error were obtained from the block averages of l_k calculated over non-overlapping intervals of about 10^8 integration steps. The diffusion coefficient was calculated from the linear fit of the knot mean-square displacements versus time cumulated over all production run. Its error was estimated from the dispersion of the diffusion coefficients calculated separately for the various runs. An analogous procedure was used to compute the average and standard deviations of the drift velocity in DC and AC fields. The standard expression for error propagation was used to compute the error on derived quantities.

2.4 Knot location

The measured knotted portion is the shortest arc on the chain which has the same topology of the whole chain. To assign a topology to open chains and arcs we closed them into a ring, using the minimally interfering closure previously developed by some of us[41].

To speed up the search for the shortest knotted portion, we applied an iterative version of the topology-preserving rectification procedure adopted in refs.[15,42]. The standard rectification scheme consists in picking a random vertex i of the ring and calculate if it can be made collinear with its neighbouring vertices $i-1$ and $i+1$ without crossing any edges of the ring. If it is possible, the vertex is eliminated. The procedure is then carried on until no more vertices can be eliminated. In our case we impose a simplification stride, s, to limit the number of subsequent vertices that can be eliminated and then carry out the standard procedure in consecutive sweeps of increasing stride, $s' = 2 * s$, until we reach a desired limiting stride $s_{max} = 20$. To reduce the uncertainty on the knot length introduced by the simplification procedure, we first identify the shortest knotted portion on the rectified chain, and then we perform again the search inside this region on the unrectified chain with a limiting stride of 2.

3 Results

3.1 Free knot diffusion

We started by characterizing the motion of knots along a polyelectrolyte chain that is stretched by pulling both ends in opposite directions with a constant force, F_s.

Specifically, we considered five knot types, namely 3_1, 4_1, 5_1, 5_2 and 7_1 knots, that are initially accommodated and equilibrated in the middle of a model DNA chain of length $L_c = 5\mu$m stretched by a force, $F_s = 10.0$pN. This force value is chosen because it falls in the typical range used in current DNA manipulation experiments with optical tweezers. As in other studies[33], the types of knots considered were chosen to provide a minimal set of simple and experimentally accessible prime knots, with a good balance of twist (3_1, 4_1 and 5_2) and torus knots (3_1, 5_1 and 7_1). We also point out that the 4_1 knot is achiral while the others are chiral.

A typical configuration of the stretched DNA chain, with the time evolution of the knotted region location is provided in Fig. 1a,b.

A relevant parameter to characterize the internal dynamics, mechanics and equilibrium properties of the knotted chains is

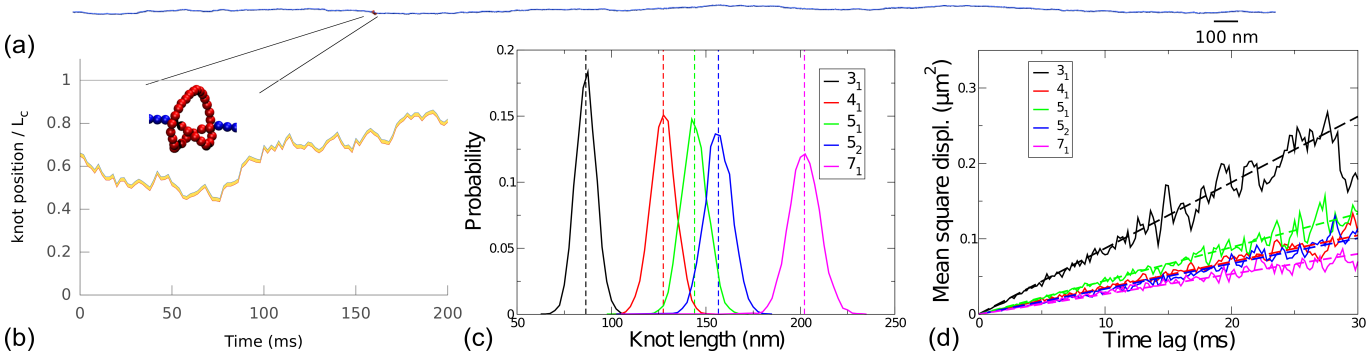

Fig. 1 Knot diffusion along a stretched DNA chain without an external field. All panels refer to model DNA chains with $L_c = 5\mu$m subjected to a stretching force $F_s = 10.0$pN. (a) Typical configuration of a trefoil-knotted (3_1) DNA chain. The knotted region is highlighted in red. (b) Typical time evolution of the boundaries of the knotted region. (c) Knot length distributions for 3_1, 4_1, 5_1, 5_2, 7_1 knots; the dashed lines mark the average values, see Table 1. (d) Time dependence of the mean-square displacement of the knot along the chain. The dashed lines indicate the linear fitting curves.

the contour length of the knotted region, l_k [30,33,43].

The distribution of l_k of the different knot types is shown in Fig. 1c along with their average values, given also in Table 1. It is seen that $\langle l_k \rangle$ increases with the nominal complexity of the knot. Such trend is, in fact, known to apply generally because it was observed in untensioned knotted rings as well as in tensioned knotted chains without electrostatic self-repulsion [33].

In all cases, the knotted region spans only a small fraction of the chain. This is a particularly interesting point which highlights the competition between several effects: the applied mechanical tension, the chain intrinsic bending rigidity and the effective one introduced by the Coulombic self-repulsion. In fact, for untensioned knotted rings it is known that knots acquire a swollen configuration spanning a sizeable fraction of the ring when the persistence length l_p exceeds the electrostatic persistence one, $l_c = q^2 \lambda_{DH}^2 / 4\pi\varepsilon_0\varepsilon_r \kappa_B T \sigma^2$ [20,44]. Tight knots are instead possible, at least as metastable states, for $l_c > l_p$. For the system under consideration $l_c = 64$nm is indeed larger, though comparable, than $l_p = 50$nm. This fact, along with the mechanical tension applied at the termini (which replaces the chain closure condition of ref. [20]) produces tight knotted configurations as shown in Fig. 1a.

The spread of the knot length distributions in Fig. 1c indicates that, although being relatively tight, knots are still capable of fluctuating substantially in length. In fact, they can also displace along the chain contour as it is illustrated in Fig. 1d which portrays time-evolution of the the mean square displacement of the center of the knotted region. The fitting lines in Fig. 1d show that the mean square displacement has an overall linear dependence on time. Therefore, although knots fluctuate in size and are subject to the three-dimensional fluctuations of the chain, their motion along the contour is compatible with a standard one-dimensional diffusive process.

Knot type	$\langle l_k \rangle$ nm	D μm^2/s	Self diffusion time ms
3_1	86.415 ± 0.055	4.19 ± 0.81	0.89 ± 0.17
4_1	127.415 ± 0.094	1.77 ± 0.31	4.57 ± 0.80
5_1	143.970 ± 0.059	2.21 ± 0.27	4.68 ± 0.58
5_2	156.60 ± 0.15	1.70 ± 0.37	7.2 ± 1.6
7_1	202.139 ± 0.058	1.32 ± 0.10	15.5 ± 1.1

Table 1 Properties of knots in tensioned DNA chains without an external electric field Average knot length, diffusion coefficient and self diffusion time for various knot types in the model DNA chains tensioned by a stretching force of 10.0pN and without an external field. The self-diffusion time is the time required by the knot to diffuse along the chain by a distance equal to the average knot length.

The corresponding diffusion coefficients, D, are provided in Table 1 along with the average knot length, and self-diffusion time.

One observes that D decreases with the increasing complexity of torus knots (3_1, 5_1 and 7_1) and that the diffusion coefficients of 5_1 and 5_2 knots are comparable. These properties are consistent with earlier results of Makarov [33] on knotted semi-flexible tensioned chains (without the electrostatic self-repulsion considered here).

In absolute terms, the values of D reported in Table 1 are between 2 and 3 times larger than those reported in experiments on much longer dsDNA filaments (from 40 to 100μm) in a buffer with polyethylene glycol and stretched by smaller forces (from 0.1 to 2.0pN) [29]. Also, the diffusion coefficients are between a half and a third of those computed numerically for longer DNA chains treated with a different model (chains

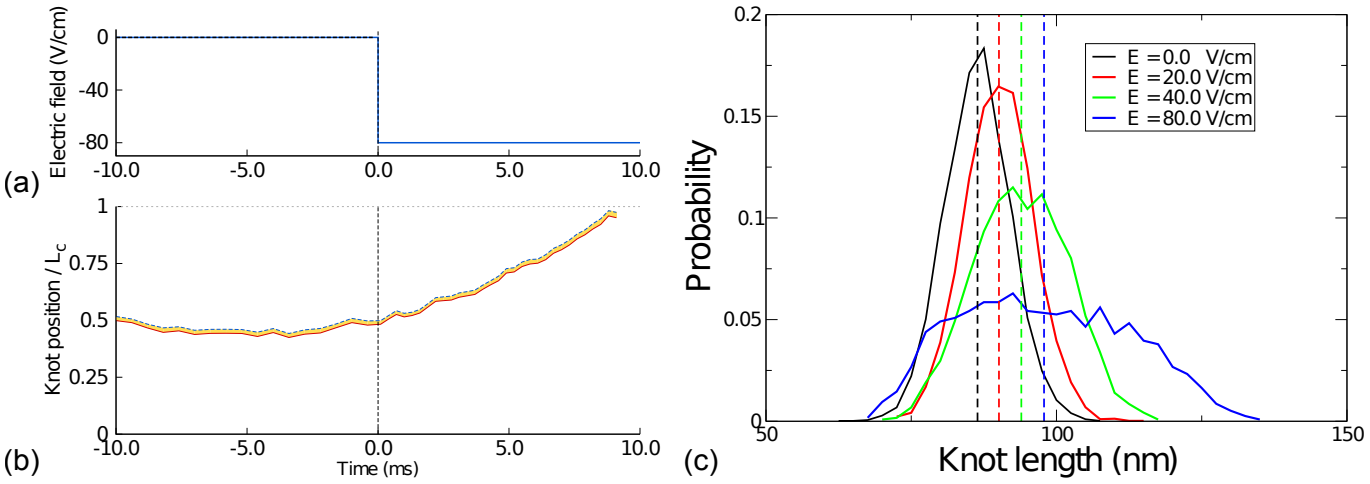

Fig. 2 Effect of a DC electric field on a trefoil knotted tensioned DNA chain. Upon switching an external field of magnitude 80V/cm at time $t = 0$, see panel (a), the knotted region slides along the chain contour in the direction of the electric force with a definite average drift velocity, see panel (b). As it is shown in the knot length distributions in panel (c), the introduction of the field midly affect the average knot lengths, which are indicated by the dashed lines.

of cylinders) which further accounted for hydrodynamic effects[31].

3.2 DC field

We proceed by studying the behavior of $3_1, 4_1, 5_1, 5_2$ and 7_1 knots in the stretched model DNA chain after introducing a uniform DC electric field of magnitude E. To prevent the chains from drifting, the mechanical tension is enforced not by applying a constant tensile force at the termini, but by fixing the latter in space so that their distance corresponds to a nominal tension of ~ 10.0pN in zero field, see Methods.

The field is collinear to the stretching direction, and its magnitude is set equal to $E \simeq 20$, 40 and 80V/cm. The corresponding total electrostatic forces acting on the chain are 5.0, 10.0 and 20.0pN, i.e. comparable with the chain tension in zero field.

We find that knots are mildly affected in their length by the electric field action and acquire a systematic drift in the direction of the electric force. Both aspects are illustrated in Fig. 2 for trefoil knots.

The dependence of the knot drift velocity, $v_{\rm drift}$, on the field strength and knot type is reported in Fig. 3a. The results are noteworthy in two respects.

First, one observes that, for any given value of the field, the drift velocities are similar across the various knot types, although torus knots (3_1, 5_1 and 7_1) velocities are systematically larger than those of twist knots (4_1 and 5_2). This effect is reminescent of what is commonly observed for macroscopic threads and ropes where twist knots are employed as stoppers because of their enhanced hindrance to sliding compared to torus knots.

The second interesting aspect regards the possibility to rely on the drift velocity and the diffusion coefficient in zero field, D, to infer an effective "frictional length", $l_{\rm friction}$ associated with the various knot types.

In fact, by modelling the stochastic motion of the knot along the chain as a one-dimensional Langevin process, one can relate the drift velocity to the effective electrostatic force acting on the knot and the underlying friction coefficient of the process:

$$v_{\rm drift} = qE l_{\rm friction} \frac{D}{\kappa_B T} \frac{1}{\sigma} . \qquad (9)$$

It should be noted that *a priori*, the effective frictional length needs not to coincide with the knot length, l_k, which measures the extent of the minimal region that (upon closure) has a definite topological state.

The value of $l_{\rm friction}$ obtained by inverting eq. 9 are shown in Fig. 3b. For each knot type, the frictional length is practically independent of the field strength. This is consistent with the fact that the average knot length l_k is also rather constant across the explored values of E and hence the self-contact effects which are arguably responsible for the topological friction are expected to be largely independent of E too.
The notable quantitative fact emerging from Fig. 3b is that $l_{\rm friction}$ is significantly smaller than l_k; typically by a factor of about 4. This indicates that only a fraction of the knotted region is effectively responsible for the topological friction.

Based on this, we believe it would be most interesting to probe $l_{\rm friction}$ experimentally (since both $v_{\rm drift}$ and D can be obtained from optical measurement) as it can provide a valuable information about key knot properties which would oth-

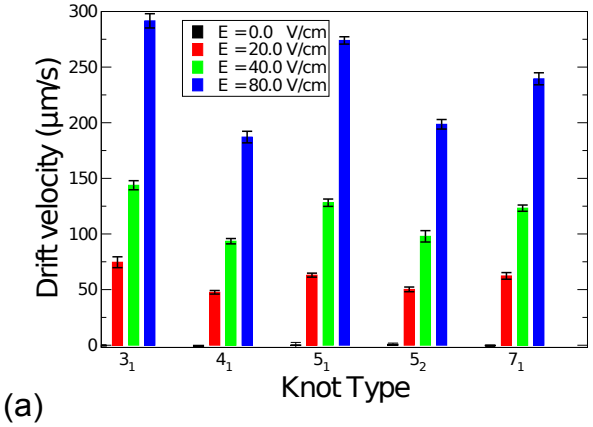

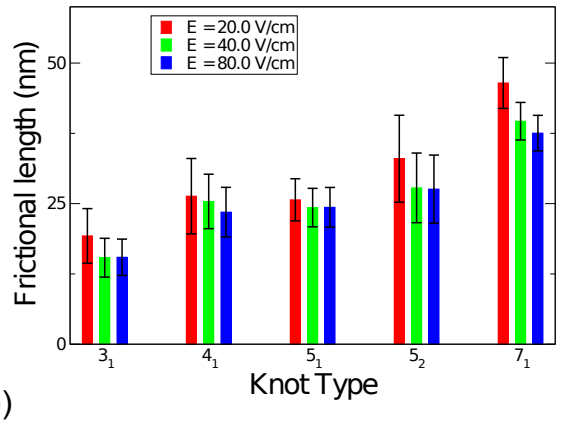

Fig. 3 Drift velocity (a) and frictional length (b) for various knot types and DC field strengths. The drift velocity was computed from the displacements of the knot center along the oriented contour at time lags of 0.1ms. This time lag was chosen because it is much smaller than the self-diffusion time of any considered knot type.

erwise not be directly accessible experimentally (such as the knot length, l_k).

3.3 AC field

We conclude the analysis of the driven motion of knots on stretched DNA chains by considering the application of a longitudinal AC field. The electric field is modulated as a square wave with amplitude equal to 80V/cm. In this way, the modulus of the applied field is, at all times, equal to the largest one used in the DC cases.

The effect of the AC field on the knot motion is illustrated in Fig. 4 which shows the knot position after the AC field is

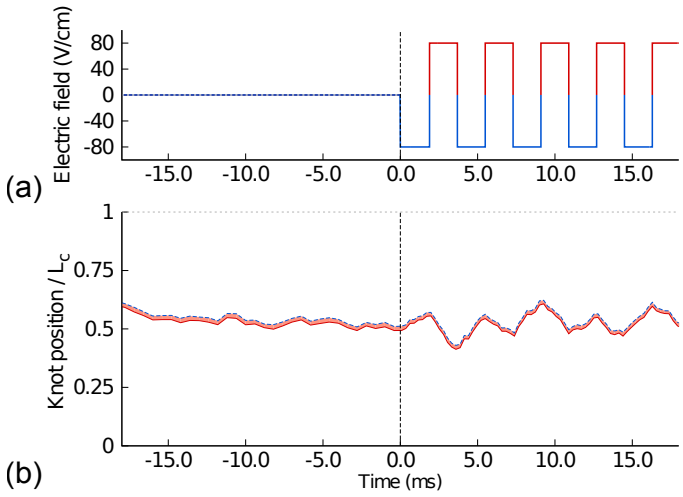

Fig. 4 Effect of an AC electric field on a knotted tensioned DNA chain. Upon switching on an AC electric field (magnitude: 80V/cm, period: 3.6ms) at time $t = 0$, see panel (a), the knotted region moves stochastically along the chain contour responding to the oscillations of the dragging field, see panel (b).

switched on at time $t = 0$. As it is apparent from the figure, the knot motion presents noticeable fluctuations during the trajectory, which indicates *a posteriori* that the applied field amplitude is not large enough to obliterate the stochastic motion.

Yet, even for this value of the field (which was chosen because it can be feasibly used in optical tweezers experiments) the AC field action does affect the knot motion in a detectable way, to the point that one can observe a striking interplay of the AC driving period and the intrinsic timescale of the knot motion.

These effects are aptly characterized by a suitable analysis of the knot velocity (identified with the velocity of its central point), and particularly the deviations of its average from zero reference value in no field. Accordingly, we computed the average knot velocity at various stages of the driving period. The latter is conveniently quantified through the cycle index, $I(t)$,

$$I(t) = -\frac{2}{E_0 \mathrm{T}} \int_0^t dt' E(t') \qquad (10)$$

where E_0 and T are, respectively, the amplitude and the period of the electric field square wave whose instantaneous value at time $t'$is indicated with $E(t')$. At time $t = 0$ the field is at the beginning of the half-period with value -80V/cm and hence the $I(t)$ index varies periodically and without discontinuities in the [0:1] range during the AC cycle by following a saw tooth profile.

The average knot drift velocity at various stages of the cycle is shown in Fig. 5 for two different driving periods. At the longest period the v_{drift}-I curves show that, albeit with an initial delay, the knot velocity can adjust to the field reversal

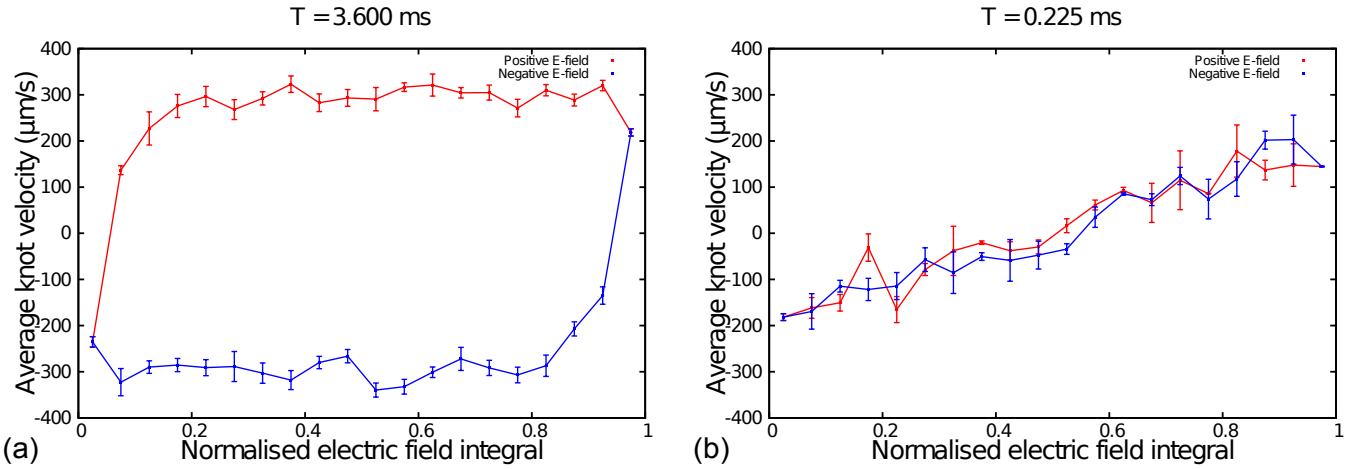

Fig. 5 Average drift velocities of a trefoil knot in a tensione DNA chain at various stages of the square-wave AC field cycle. The magnitude of the external field is 80V/cm, as in Fig 4a. Panels (a) and (b) refer to AC periods of 3.6ms and 0.225ms, respectively.

and attain its steady-state limiting value, see panel a. Reaching such steady state becomes impossible if the driving period is too short, see panel b.

It is readily noticed from Fig. 5 that the area enclosed by the closed curve, which is proportional to the work done by the field on the knot, is sizeable for the 3.6ms period and negligible for the 0.225ms. This difference is partly due to the fact that longer periods involve power dissipation over longer times.

To account for this effect we computed the dissipated power as the time-average of the product of the drift velocity and the applied field. Given the substantial stretching of the chain, we considered for simplicity the drift velocity along the contour in place of its projection on the stretching/field direction. Finally, for each knot we normalised the power by its value at the largest period (~ 3.6ms).

The normalised dissipated power is shown in Fig. 6 for 3_1 and 4_1 knots as a function of the AC period. One observes that both curves have a striking downward trend for decreasing AC period. The dissipated power is practically zero for periods smaller than about 0.25ms for both 3_1 and 4_1 knots.

The associated half period (during which the field acts consistently, before its directionality is reverse) of 0.5ms provides an intrinsic relaxation time for the knots. In fact, only for longer driving periods, knots can adjust and follow the repeated changes of directionality. By comparison with the data in Table 1 it is noticed that for both 3_1 and 4_1 knots the relaxation timescale is a fraction of the self-diffusion time (which bounds it from above since it provides a timescale over which the knot position along the chain is completely renewed).

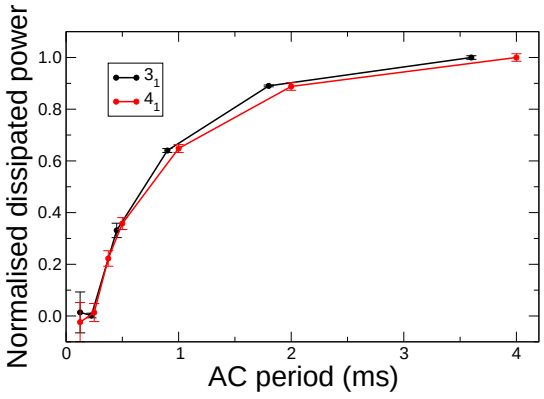

Fig. 6 AC dissipation for 3_1 and 4_1 knots in AC electric fields. The dissipated power for 3_1 and 4_1 knots in tensioned DNA chains is computed as a function of the AC electric field period and, for ease of interpretation is normalised to the dissipated power at the slowest period, $T = 3.6$ms. Each data point is averaged over at least 100 AC cycles collected over different initial conditions.

3.4 Simulations with explicit counterions

The results presented so far were obtained for a model system where the action of counterions in solution was implicitly taken into account through the Debye-Hückel screened electrostatics.

To confirm the generality and robustness of the observed phenomenology we have repeated the analysis for knotted polyelectrolyte chains in the presence of explicit counterions. To keep the computational cost at a manageable level we con-

sider chains parametrised as before except for the chain length and bead charge which are reduced to $N = 150$ beads and $q = -3$e, respectively. Each chain is placed within a periodic box with sides equal to 37.5, 37.5 and 375.0nm. To ensure the overall system neutrality, we add to the system 450 monovalent counter-ions with same size and mass as the chain beads, corresponding to a nominal salt concentration of 1.4mM and $\lambda_{DH} \sim 8$nm. All charges in the system, except the nearest neighbours along the chain, interact via the standard unscreened Coulomb interaction.

Note that the electrostatic persistence length[44] is $l_c = 64$nm which is larger than $l_p = 50$nm, similarly to the DNA case considered before. Accordingly, based on the criteria of Dommersnes *et al.*[20] knots are expected to be tight in the absence of a stretching force.

The model system was first studied by characterizing the free motion of 3_1 knots along the chains in zero electric field with their termini fixed at a separation of 325nm, corresponding to the same nominal tension of 10.0pN applied to the model DNA. The average knot length and self-diffusion time were found to be respectively equal to 35nm and 0.3ms, see SI Fig. 1.

The DC response was studied by introducing a longitudinal electric field producing a total dragging force of 20.0pN (again equal to that considered for DNA). Despite the reduced beads charge and the backflow of the counterions, the knot was found to acquire a net motion in the direction of the electric force, as for the DNA system without counterions, see SI Fig. 2.

The accord with earlier findings extended to the AC behaviour as well, as shown in Fig. 7. In particular, it is seen that the dissipated power versus driving period has a trend analogous to the one of Fig. 6. In absolute terms, the characteristic cutoff time for this system with reduced bead charges and explicit counterions is equal to 0.01ms and hence substantially smaller than for the model DNA case (0.25ms). In relative terms, the 0.01ms relaxation time is now also appreciably smaller than the upper bound provided by the self-diffusion time (0.3ms).

We plan to explore more systematically in the future the effect of the counterion backflow on the motion of knots on polyeletrolytes with different beads charge and mass than considered here.

4 Conclusions

The effect of DC and AC electric fields on the dynamics of entangled polymers was investigated theoretically and numerically for mechanically-stretched polyelectrolytes. Specifically, we considered knotted DNA chains under mechanical tension and subject to the action of an external electric field.

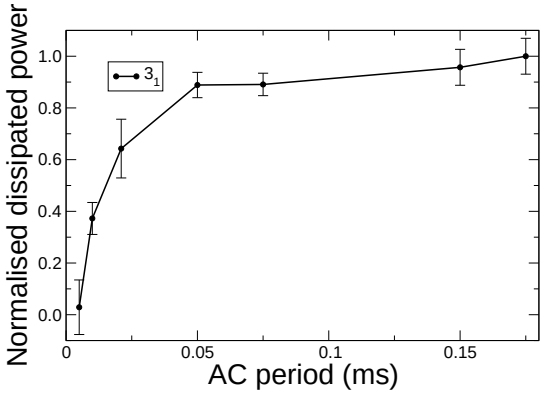

Fig. 7 AC dissipation curves for a trefoil knot in a model tensioned polyeletrolyte chain with explicit counterions. The dissipated power for the 3_1 knot in tensioned DNA chains is computed for AC electric field with different period and, for ease of interpretation is normalised to the dissipated power at the slowest period. Each data point is averaged over at least 100 AC cycles collected over different initial conditions.

The system is interesting *a priori* because of the expected interplay of several competing effects on the motion of the knotted region. These include the bending forces and electrostatical self-interaction of the chain which may lead the knot to tighten or to swell depending to the ratio of their persistence lengths, as demonstrated in ref[20], and the mechanical tension to which the chain is subjected. Our study investigated in particular the tight knots regime.

It is found that all considered knot types, including twist ones, maintain their ability to slide along the chain under an external electric field. In particular, knots are dragged in the direction of the electric force with a field-dependent drift velocity.

By measuring the friction associated to the drift velocity one can define a previously unexplored characteristic knot lengthscale, the frictional length. This length, which could also be computed from experimental measurements, is smaller than the nominal knot length since it captures the extent of self-interactions within the knotted region.

The rich phenomenology of the dynamics of self-entangled polyelectrolytes was aptly exposed by applying AC fields of various frequencies. In particular, for sufficiently low (and experimentally accessible) AC frequencies, the knot motion presents the typical signatures of dynamical systems with memory, such as a lag time in following the time-modulation of the external fields. For frequencies higher than a critical value, the knot becomes completely unable to follow the ex-

ternal field which does not do a net work on the knot. The transition from the dissipative regime to the "frozen" one can be rationalised in terms of a spontaneous, intrinsic relaxation time associated to the motion of the knots along the chain.

5 Acknowledgements

We are indebted with Greg Buck, Giovanni Bussi, Enzo Orlandini and Angelo Rosa for valuable discussions. M.D.S. and C.M. acknowledge support from the Italian Ministry of Education grant PRIN Nr. 2010HXAW77. L.T. acknowledges support from the Slovenian Agency for Research and Development, Grant Nr. J1-4134.

References

1 M. Delbrück, Mathematical problems in biological sciences, 1962, p. 55.
2 E. Orlandini and S. G. Whittington, *Rev. Mod. Phys.*, 2007, **79**, 611.
3 M. Kardar, *The European Physical Journal B-Condensed Matter and Complex Systems*, 2008, **64**, 519–523.
4 A. Grosberg, *Polymer Science Series A*, 2009, **51**, 70–79.
5 A. Grosberg, *Physical review letters*, 2000, **85**, 3858–3861.
6 V. Katritch, W. K. Olson, A. Vologodskii, J. Dubochet and A. Stasiak, *Phys. Rev. E*, 2000, **61**, 5545–5549.
7 O. Farago, Y. Kantor and M. Kardar, *Europhys. Lett.*, 2002, **60**, 53–59.
8 P. Virnau, Y. Kantor and M. Kardar, *Journal of the American Chemical Society*, 2005, **127**, 15102–15106.
9 B. Marcone, E. Orlandini, A. Stella and F. Zonta, *Physical Review E*, 2007, **75**, 041105.
10 M. Baiesi, E. Orlandini, A. L. Stella and F. Zonta, *Phys. Rev. Lett.*, 2011, **106**, 258301.
11 D. Marenduzzo, C. Micheletti and E. Orlandini, *Journal of Physics: Condensed Matter*, 2010, **22**, 283102.
12 D. Meluzzi, D. Smith and G. Arya, *Annual review of biophysics*, 2010, **39**, 349–366.
13 C. Micheletti, D. Marenduzzo and E. Orlandini, *Physics Reports*, 2011, 1–73.
14 A. Rosa, M. Di Ventra and C. Micheletti, *Physical review letters*, 2012, **109**, 118301.
15 W. Taylor, *Nature*, 2000, **406**, 916–919.
16 D. Bölinger, J. I. Sułkowska, H.-P. Hsu, L. A. Mirny, M. Kardar, J. N. Onuchic and P. Virnau, *PLoS computational biology*, 2010, **6**, e1000731.
17 P. Virnau, A. Mallam and S. Jackson, *Journal of Physics: Condensed Matter*, 2011, **23**, 033101.
18 T. Škrbić, C. Micheletti and P. Faccioli, *PLoS computational biology*, 2012, **8**, e1002504.
19 L. Tubiana, A. Rosa, F. Fragiacomo and C. Micheletti, *Macromolecules*, 2013, **46**, 3669–3678.
20 P. G. Dommersnes, Y. Kantor and M. Kardar, *Physical Review E*, 2002, **66**, 031802.
21 A. Rosa, E. Orlandini, L. Tubiana, C. Micheletti, *Macromol.*, 2011, **44**, 8668–8680.
22 J. Tang, N. Du and P. S. Doyle, *Proceedings of the National Academy of Sciences*, 2011, **108**, 16153–16158.
23 E. Orlandini, A. L. Stella, C. Vanderzande and F. Zonta, *J. Phys. A: Math. Theor.*, 2008, **41**, 122002.
24 P. Szymczak, *Biochemical Society transactions*, 2013, **41**, 620–624.
25 L. Huang and D. E. Makarov, *The Journal of chemical physics*, 2008, **129**, 121107.
26 F. Tessier, J. Labrie and G. Slater, *Macromolecules*, 2002, **35**, 4791–4800.
27 D. Marenduzzo, E. Orlandini, A. Stasiak, D. W. Sumners, L. Tubiana and C. Micheletti, *Proceedings of the National Academy of Sciences of the United States of America*, 2009, **106**, 22269–22274.
28 D. Marenduzzo, C. Micheletti, E. Orlandini and D. W. Sumners, *Proceedings of the National Academy of Sciences of the United States of America*, 2013, **110**, 20081–20086.
29 X. Bao, H. Lee and S. Quake, *Physical review letters*, 2003, **91**, 265506.
30 Y. Arai, R. Yasuda, K. Akashi, Y. Harada, H. Miyata, T. Kinosita and H. Itoh, *Nature*, 1999, **399**, 446–448.
31 A. Vologodskii, *Biophys. J.*, 2006, **90**, 1594.
32 R. Matthews, A. Louis and J. Yeomans, *EPL (Europhysics Letters)*, 2010, **89**, 20001.
33 L. Huang and D. E. Makarov, *The Journal of Physical Chemistry A*, 2007, **111**, 10338–10344.
34 X. Zheng and A. Vologodskii, *Phys. Rev. E*, 2010, **81**, 041806.
35 R. Matthews, A. A. Louis and C. N. Likos, *ACS macro letters*, 2012, **1**, 1352–1356.
36 Y. V. Pershin and M. Di Ventra, *Advances in Physics*, 2011, **60**, 145–227.
37 M. Zwolak and M. Di Ventra, *Rev. Mod. Phys.*, 2008, **80**, 141–165.
38 K. Kremer and G. S. Grest, *J. Chem. Phys.*, 1990, **92**, 5057.
39 S. J. Plimpton, *J. Comp. Phys.*, 1995, **117**, 1–19.
40 C. Maffeo, R. Schöpflin, H. Brutzer, R. Stehr, A. Aksimentiev, G. Wedemann and R. Seidel, *Phys. Rev. Lett.*, 2010, **105**, 158101.
41 L. Tubiana, E. Orlandini and C. Micheletti, *Progress of Theoretical Physics Supplement*, 2011, **191**, 192–204.
42 K. Koniaris and M. Muthukumar, *Phys. Rev. Lett.*, 1991, **66**, 2211–2214.
43 A. M. Saitta, P. D. Soper, E. Wasserman and M. L. Klein, *Nature*, 1999, **399**, 46–48.
44 T. Odijk, *Journal of Polymer Science: Polymer Physics Edition*, 1977, **15**, 477–483.